Projected shell model study of yrast states of neutron-deficient odd-mass Pr nuclei

A. Ibáñez-Sandoval* and M. E. Ortiz
Instituto de Física, Universidad Nacional Autónoma de México, Apartado Postal 20-364, 01000 México Distrito Federal, México

V. Velázquez
Facultad de Ciencias, Universidad Nacional Autónoma de México, Apartado Postal 70-542, 04510 México Distrito Federal, México

A. Galindo-Uribarri
Physics Division, Oak Ridge National Laboratory, Oak Ridge, Tennessee 37831, USA

P. O. Hess
Instituto de Ciencias Nucleares, Universidad Nacional Autónoma de México, Apartado Postal 70-543, 04510 México Distrito Federal, México

Y. Sun
Department of Physics, Shanghai Jiao Tong University, Shanghai 200240, People's Republic of China
Institute of Modern Physics, Chinese Academy of Sciences, Lanzhou 730000, People's Republic of China
Department of Physics and Astronomy, University of Tennessee, Knoxville, Tennessee 37996, USA
(Received 4 October 2010; published 9 March 2011)

A wide variety of modern instruments allow us to study neutron-deficient nuclei in the $A = 130$ mass region. Highly deformed nuclei have been found in this region, providing opportunities to study the deformed rotational bands. The description of the ^{125,127,129,131,133}Pr isotopes with the projected shell model is presented in this paper. Good agreement between theory and experiment is obtained and some characteristics are discussed, including the dynamic moment of inertia $\mathcal{J}^{(2)}$, kinetic moment of inertia $\mathcal{J}^{(1)}$, the crossing of rotational bands, and backbending effects.

DOI: 10.1103/PhysRevC.83.034308 PACS number(s): 21.10.Re, 27.60.+j, 21.60.Cs

I. INTRODUCTION

The study of neutron-deficient nuclei in the A-130 mass region has been an interesting subject in nuclear structure physics [1]. In this mass region a highly-deformed band was observed first in ^{132}Ce [2], where a series of γ-ray transitions with an energy separation of approximately 70 keV were found. This band was quantitatively described by the projected shell model (PSM) [3]. ^{132}Ce has played a central role in the investigation of superdeformed structure of A-130 nuclei. The major interest in studying A-130 nuclei is to understand the different contributions of neutrons and protons. In these nuclei both neutrons and protons occupy the high-j $h_{11/2}$ intruder orbitals. In odd-mass Pr nuclei, for example, the neutron orbitals evolve in the middle of the $h_{11/2}$ shell, while the proton Fermi surface lies in the lower part of the shell. Rotation alignment of the $h_{11/2}$ protons would drive the nucleus to a prolate shape, while alignment of $h_{11/2}$ neutrons would produce an opposite effect in deformation. This poses an interesting situation with strong competition of neutrons and protons in a fast rotating system.

The yrast bands in odd-Pr nuclei are characterized by a decoupled $h_{11/2}$ proton configuration for low spin states and rotation alignment of an additional pair of nucleons for high spin states [4–7]. These bands have been investigated with the cranked shell model (CSM) in which the calculations predicted that the band crossing occurs around $\hbar\omega \approx 0.5$ MeV while the experimental data suggested a lower value around $\hbar\omega \approx 0.4$ MeV [6,8]. The origin of the crossing has not been well understood despite many intensive studies. There have been suggestions that it is attributed to the neutron alignment [6,9–11], whereas other studies indicated an alignment of a pair of protons [5,12]. We may thus conclude that the configuration assignment for the high spin states in these odd Pr nuclei and the nature of the rotation alignment are still open questions. In the past two decades, the projected shell model [13] has been applied to study the structure of high spin states. Different from the CSM, which works in the intrinsic frame, the PSM transforms the configurations to the laboratory frame by using the angular momentum projection, and further mixes them in the laboratory frame by diagonalizing a two-body Hamiltonian. Mixing of the configurations in the laboratory frame removes ambiguities in the band-crossing region in the CSM, which is a well-known problem of the cranking approximation first pointed out by Hamamoto [14]. Thus the PSM is in principle better suited for the study of the band-crossing phenomenon. The PSM has been extensively applied to study superdeformed as well as normal deformed bands in different mass regions [3,15–19]. The recent PSM calculations for the even-even $^{124-130}$Ce isotopes [20,21], the $^{98-102}$Sr and $^{100-104}$Zr isotopes [22], the neutron-rich $^{154-160}$Nd and $^{156-162}$Sm isotopes [23], as well as for very heavy nuclei [24] and light nuclei [25], have

*Also at Escuela Superior de Ingeniería Mecánica y Eléctrica Unidad Zacatenco, Instituto Politécnico Nacional, 07738, México Distrito Federal, México.

shown satisfactory agreement with experimentally observed yrast bands and demonstrated the ability of the PSM to describe the backbending phenomenon.

The purpose of the present work is to carry out a systematical study on the yrast bands in the odd-mass $^{125-133}$Pr nuclei, a set of isotopes which are difficult to describe. We demonstrate that it is possible to reproduce the experimental data with the PSM by using the same set of parameters as in the even-even nuclei in the $A = 130$ mass region, and we further provide detailed analysis for the structure of these isotopes. The paper is arranged as follows. An outline of the PSM is given in Sec. II. Theoretical discussion and comparison with experimental data are presented in Sec. III. Finally, conclusions are drawn in Sec. IV.

II. OUTLINE OF THE PROJECTED SHELL MODEL

The PSM has been developed as a shell model truncation scheme which is implemented in a deformed single-particle basis [13]. Pairing correlations are included in this basis, which is constructed by the quasiparticle (qp) states obtained from a Nilsson + BCS calculation. The shell model truncation is carried out by considering the low-lying multi-qp configurations around the Fermi levels. We then use the angular-momentum-projection method to restore the rotational symmetry violated in the deformed basis. Finally, the two-body Hamiltonian is diagonalized in the projected basis.

The following set of multi-qp configurations is used for odd-proton nuclei:

$$|\Phi_k\rangle = \{a_\pi^\dagger|0\rangle, a_\pi^\dagger a_{\nu 1}^\dagger a_{\nu 2}^\dagger|0\rangle\}, \tag{1}$$

where $a^\dagger$'s are the qp creation operators and k labels each configuration. The states are written in the Nilsson + BCS representation, with ν's (π's) representing the neutron (proton) Nilsson quantum numbers, which run over low-lying orbitals, and $|0\rangle$ the qp vacuum state. The 3-qp states are formed by one quasiproton plus a pair of quasineutrons. The inclusion of the 3-qp configurations is important for odd-mass nuclei for a description of the band-crossing phenomenon which is caused by a rotation alignment of a pair of quasineutrons.

The Hamiltonian employed in the calculation is [13]

$$\hat{H} = \hat{H}_0 - \frac{\chi}{2}\sum_\mu \hat{Q}_\mu^+ \hat{Q}_\mu - G_M \hat{P}^+\hat{P} - G_Q \sum_\mu \hat{P}_\mu^+ \hat{P}_\mu, \tag{2}$$

where H_0 is the spherical single-particle Hamiltonian which contains a proper spin-orbit force. The second term in Eq. (2) is the quadrupole-quadrupole (QQ) interaction and χ represents its strength, which is determined by the self-consistent relation between the input quadrupole deformation ϵ_2 and the one resulting from the HFB procedure [13,26]. The last two terms are the monopole and quadrupole pairing interactions, respectively. The strengths of the monopole pairing interactions are given by

$$G_M^\nu = \left(19.60 + 15.7\frac{N-Z}{A}\right)\frac{1}{A}, \quad G_M^\pi = 19.60\frac{1}{A}, \tag{3}$$

and that for the quadrupole pairing interaction is related to the monopole pairing by

$$G_Q = \gamma G_M, \tag{4}$$

with $\gamma = 0.16$. These strengths are the same as those in Ref. [3], which have been tested by other PSM calculations for this mass region [20,21]. As noticed by Dufour and Zuker [27], these interactions represent the essence of the most important correlations in the low-lying nuclear spectrum.

The Hamiltonian (2) is diagonalized in the shell model space spanned by $\hat{P}^I_{MK}|\Phi_k\rangle$, where the $\hat{P}^I_{MK}$ is the angular-momentum-projection operator and $|\Phi_k\rangle$ the multi-qp states of Eq. (1). The eigenvalue equation for each spin I is given by

$$\sum_{k'}\left(H^I_{kk'} - E^{I\alpha}N^I_{kk'}\right)F^{I\alpha}_{k'} = 0, \tag{5}$$

where α enumerates the states with the same spin. The normalization is chosen such that

$$\sum_{kk'} f^\alpha_k N_{kk'} f^{\alpha'}_{k'} = \delta_{\alpha\alpha'}, \tag{6}$$

and the Hamiltonian matrix elements $H^I_{kk'}$ and the norm matrix elements $N^I_{kk'}$ in (5) are

$$H^I_{kk'} = \langle\Phi_k|\hat{H}\hat{P}^I_{KK'}|\Phi_{k'}\rangle, \quad N^I_{kk'} = \langle\Phi_k|\hat{P}^I_{KK'}|\Phi_{k'}\rangle. \tag{7}$$

The band energies are obtained when we calculate the expectation values of the Hamiltonian with respect to a "rotational" band k, which are obtained from each angular-momentum-projected state in (1). Thus the rotational energy of a band k is defined as

$$E_k(I) = \frac{\langle\Phi_k|\hat{H}\hat{P}^I_{KK}|\Phi_k\rangle}{\langle\Phi_k|\hat{P}^I_{KK}|\Phi_k\rangle} = \frac{H^I_{kk}}{N^I_{kk}}, \tag{8}$$

which are the diagonal elements in Eq. (7) with respect to a projected multi-qp state k. A diagram containing rotational energies of various bands as a function of spin I is called a band diagram [13]. From band diagrams we can study the properties such as the crossing of rotational bands, which we will discuss in the following sections.

III. CALCULATIONS AND COMPARISON WITH DATA

To carry out calculations, we use the PSM code published in Ref. [28]. First, a deformed basis is constructed from the standard Nilsson model, and the κ and μ parameters in the Nilsson potential are taken from Ref. [29]. We consider three major shells ($N = 3$, 4, and 5) for both neutrons and protons. The parameters of the basis deformation (ϵ_2 and ϵ_4) and γ in Eq. (4) for each nucleus are given in Table I. The deformation parameters are very close to but slightly different from the values given in Ref. [30]. We note that the present calculation is of the shell model type which uses the deformed potential with suitable input parameters to generate a model basis. Different configurations (one- and three-quasiparticle states) are built within the chosen basis. Although the quasiparticle vacuum state is obtained with a fixed deformation, mixing of the multi-qp configurations can introduce dynamically some effects, such as those caused by qp alignments. These

TABLE I. Parameters used in the calculation.

	^{125}Pr	^{127}Pr	^{129}Pr	^{131}Pr	^{133}Pr
ϵ_2	0.300	0.283	0.267	0.234	0.194
ϵ_4	0.00	0.00	0.027	0.027	0.027
γ	0.16	0.16	0.20	0.20	0.20

additional treatments (the construction of projected multi-qp states and the configuration mixing) go beyond the usual mean-field methods, and therefore our deformed states are not necessarily the same as those in other models.

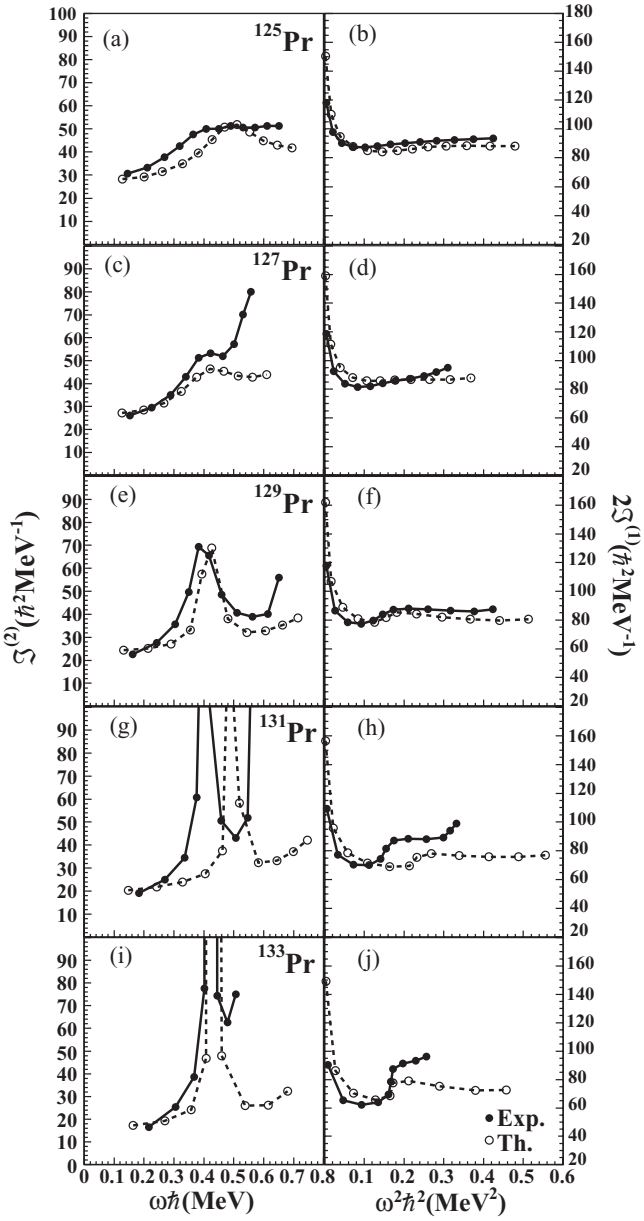

FIG. 1. Comparison between theory and experiment. (a), (c), (e), (g), (i): Dynamical moment of inertia $\mathcal{J}^{(2)}$ ($\hbar^2$ MeV^{-1}), and (b), (d), (f), (h), (j): Twice the kinetic moment of inertia $\mathcal{J}^{(1)}$ ($\hbar^2$ MeV^{-1}).

In the present work, the shell model space is truncated in such a way that only states within an energy window around the Fermi surface are selected. This determines the size of the basis space $|\Phi_k\rangle$. The energy windows that we used in the calculation are 3.5 MeV for 1-qp states and 6.5 MeV for 3-qp states. Finally, the basis states are projected to good angular momentum states, and the projected basis is used to diagonalize the shell model Hamiltonian. In this way, we obtain the energy spectra which are compared to the experimental data.

A. Backbending of moment of inertia in yrast bands

The backbending in moment of inertia, observed in the rotational spectra of deformed nuclei, carries important information on the interplay between the ground band and bands with alignment of a pair of quasiparticles. Thus, an yrast sequence is formed by states of both bands such that the lower spin states are mainly of the ground band, and the major component of the higher spin states belongs to the bands with aligned quasiparticles. In Fig. 1, we compare the PSM results with experimental data for the $^{125-133}$Pr isotopes. We plot the dynamical moment of inertia $\mathcal{J}^{(2)}$ as a function of the rotational frequency $\hbar\omega$ and twice the kinetic moment of inertia $\mathcal{J}^{(1)}$ as a function of $\hbar^2\omega^2$. These quantities are defined as

$$\mathcal{J}^{(2)} = \frac{4}{E_\gamma(I) - E_\gamma(I-2)}, \qquad 2\mathcal{J}^{(1)} = \frac{(2I-1)}{\omega}, \tag{9}$$

where the transition energy $E_\gamma = E(I) - E(I-2)$ is related to the rotational frequency through

$$\hbar\omega = \frac{E_\gamma}{\sqrt{(I+1)(I+2) - K^2} - \sqrt{(I-1)I - K^2}}. \tag{10}$$

As one can see from Fig. 1, the comparison between theory and experiment is overall satisfactory. In the right column of the figure, the kinetic moments of inertia of the isotopes are reproduced almost perfectly, except for ^{131}Pr where the rise of $\mathcal{J}^{(1)}$ in theory is shifted to a higher rotational frequency. The dynamical moment of inertia $\mathcal{J}^{(2)}$ is a very sensitive quantity as it describes the variation of $\mathcal{J}^{(1)}$. For this quantity, the results obtained for ^{125,127}Pr reproduce the observed backbending effects [see Figs. 1(a) and 1(c)] as seen

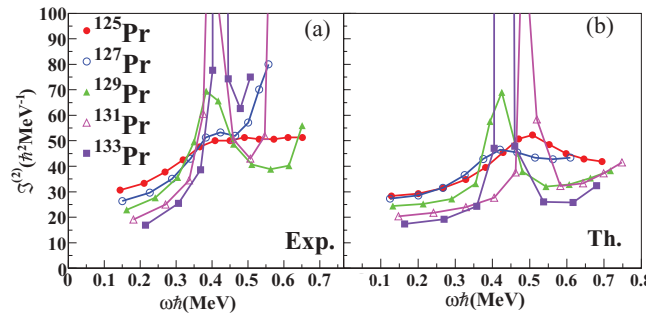

FIG. 2. (Color online) Comparison between theory and experiment for dynamical moment of inertia $\mathcal{J}^{(2)}$ ($\hbar^2$ MeV^{-1}) for all isotopes. (a) Experimental data. (b) The PSM calculation.

from the experimental data [7,8]. Nevertheless, the change of $\mathcal{J}^{(2)}$ for ^{125}Pr is predicted to occur at $\hbar\omega \approx 0.5$ MeV while experimentally it occurs at $\hbar\omega \approx 0.4$ MeV, which still can be considered as a good agreement with experiment. In the case of ^{127}Pr the change of $\mathcal{J}^{(2)}$ with rotational frequency coincides with the experimental data, with the observed value at $\hbar\omega \approx 0.4$ MeV. However, deviations of the theoretical $\mathcal{J}^{(2)}$ from the data are seen at the highest spin states. For ^{129}Pr, the PSM reproduces very well the experimental data [see Fig. 1(e)]. The change of $\mathcal{J}^{(2)}$ with rotational frequency is predicted correctly at $\hbar\omega \approx 0.4$ MeV.

The experimental data for ^{131,133}Pr are taken from Refs. [8,31]. For these two isotopes we used the original Nilsson κ and μ parameters taken from Ref. [32]. For ^{131}Pr the PSM predicts that the change of rotational frequency occurs at $\hbar\omega \approx 0.5$ MeV, while it is observed around $\hbar\omega \approx 0.4$ MeV [see Fig. 1(g)]. For ^{133}Pr the PSM predicts a change in the rotational frequency at around $\hbar\omega \approx 0.44$ MeV, while it is observed at $\hbar\omega \approx 0.43$ MeV, which is very good [see Fig. 1(i)].

Comparing all the experimental dynamical moments of inertia $\mathcal{J}^{(2)}$, we see clearly that $\mathcal{J}^{(2)}$ increases with decreasing N at low frequencies [see Fig. 2(a)]. This general behavior is correctly reproduced by the theoretical calculations of the PSM [see Fig. 2(b)]. This is also consistent with the results reported by Smith *et al.* [8] for the ^{127,129,131}Pr isotopes. This characteristic is understood to relate with the increase in the associated deformation of all the $\pi h_{11/2}$ bands while decreasing N. In fact, the PSM calculations employed varying deformation parameters from $\epsilon_2 = 0.194$ in the heavier ^{133}Pr isotope to $\epsilon_2 = 0.300$ in the lighter ^{125}Pr isotope.

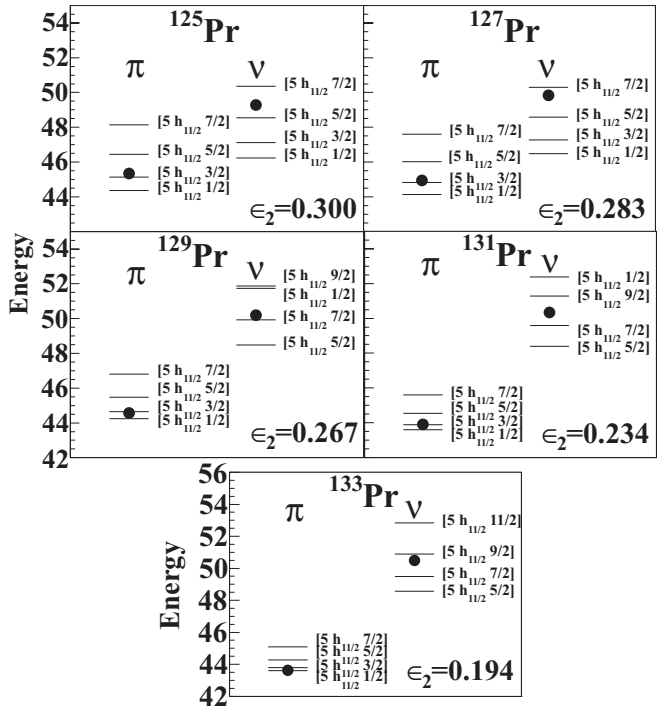

FIG. 3. Deformed single-particle energy levels for protons and neutrons near the Fermi level represented by the closed circle.

B. Band diagram analysis

The variation and backbending in moments of inertia as shown above correspond to rotation alignment of quasiparticles in particular orbitals. For odd-mass nuclei, it is phenomenologically associated with crossings between bands with 1- and 3-qp configurations. In our present case, 1-qp configurations are those from the deformed proton $h_{11/2}$ orbit, while 3-qp ones consist of these proton 1-qp configurations plus a pair of $h_{11/2}$ neutrons. Thus before we analyze the

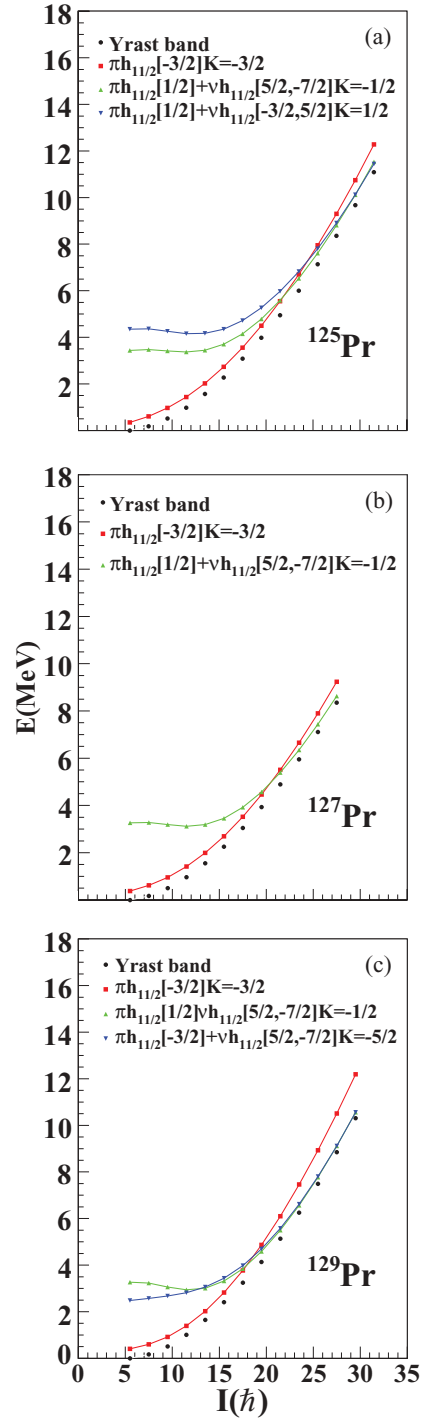

FIG. 4. (Color online) Band diagrams for $^{125-129}$Pr.

structure of the bands, it is useful to look at the deformed single-particle levels.

Figure 3 shows the single-particle levels for protons and neutrons which contribute to the 3-qp bands corresponding to the region of the backbendings. The Nilsson states have the following spherical components: $N = 5, l = h, j = 11/2$, and $m = 7/2,\ 3/2,\ 1/2,\ 5/2,\ 9/2$, which can be represented as $[5h_{11/2}7/2]$, $[5h_{11/2}3/2]$, $[5h_{11/2}1/2]$, $[5h_{11/2}5/2]$, and $[5h_{11/2}9/2]$, respectively. For the case of the proton single-particle levels there are mainly three levels that contribute in the backbending region, which are $[5h_{11/2}5/2]\pi$, $[5h_{11/2}3/2]\pi$, and $[5h_{11/2}1/2]\pi$. These levels are closer when the number of neutrons is increased, reflecting a weaker splitting of the single-particle levels with a smaller deformation. For ^{125,127}Pr there are two neutron single-particle levels $[5h_{11/2}7/2]\nu$ and $[5h_{11/2}5/2]\nu$, which contribute in the backbending region. In the case of ^{129}Pr there are three neutron single-particle levels $[5h_{11/2}9/2]\nu$, $[5h_{11/2}1/2]\nu$, and $[5h_{11/2}7/2]\nu$ which are important. For ^{131,133}Pr we have only two neutron single-particle levels $[5h_{11/2}9/2]\nu$ and $[5h_{11/2}7/2]\nu$ which are relevant to the discussion.

The band diagrams help us to understand the backbending effects which are present in the odd-Pr nuclei. In Figs. 4 and 5, the band diagrams for the ^{125,127,129,131,133}Pr isotopes are shown. We have marked each band with the corresponding qp configuration. In the calculation, our configuration space is built by many more qp states, but we only show in each diagram the most important ones.

In these diagrams for ^{125,127,129,131}Pr, we can see that the low spin states in the yrast bands are represented by a quasiproton $K = 3/2$ state from $\pi h_{11/2}$. This configuration suggests that the low spin states are based on the decoupled $h_{11/2}$ protons, and in this way the first proton alignment is blocked. These results are in agreement with the experimental assignment. In the case of ^{133}Pr, the low spin states are represented by a quasiproton $K = 1/2$ state from $\pi h_{11/2}$, which is different from the results reported in Refs. [4–7].

For the case of ^{125}Pr the band crossing in the yrast band occurs approximately at $I = 47/2^-$. The band which generates this crossing is a 3-qp state consisting of an $h_{11/2}[1/2]$ quasiproton plus a pair of quasineutrons, $h_{11/2}[5/2,-7/2]$. The PSM predicts another band crossing at $I = 63/2^-$, which is caused by a 3-qp state of an $h_{11/2}[1/2]$ quasiproton plus a pair of quasineutrons, $h_{11/2}[-3/2, 5/2]$ [see Fig. 4(a)]. In ^{127}Pr, the crossing is predicted at $I = 43/2^-$ by a 3-qp band also. This band has a configuration of a quasiproton state $h_{11/2}[1/2]$ plus a pair of quasineutrons, $h_{11/2}[5/2, -7/2]$ [see Fig. 4(b)]. For ^{129}Pr, we can see that the crossing occurs at $I = 39/2^-$. The crossing band is identified as a 3-qp band which has a configuration of a quasiproton state $h_{11/2}[1/2]$ plus a pair of quasineutrons, $h_{11/2}[5/2, -7/2]$. A third band crossing is predicted at $I = 59/2^-$. This band is generated by a

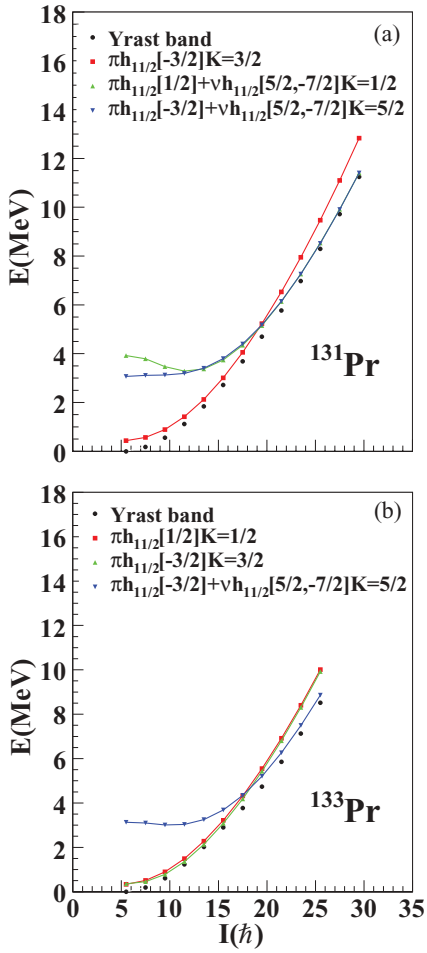

FIG. 5. (Color online) Band diagrams for $^{131-133}$Pr.

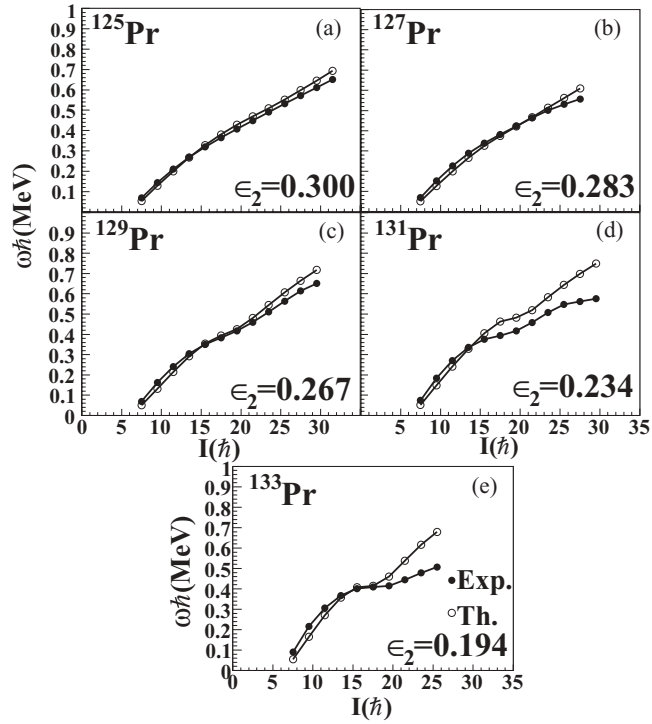

FIG. 6. Alignment diagrams for ^{125,127,129,131,133}Pr, where the spin I is plotted against the rotational frequency ω. The calculations of alignments are compared with the experimental data.

quasiproton state $h_{11/2}$[-3/2] plus a pair state of quasineutrons, $h_{11/2}[5/2, -7/2]$ [see Fig. 4(c)].

In the last two isotopes, ^{131,133}Pr, it is possible to see three configurations in each yrast band [see Figs. 5(a) and 5(b)]. In ^{131}Pr the crossing occurs at $I = 39/2^-$ which is generated by 3-qp band that has a configuration of a quasiproton state $h_{11/2}[1/2]$ plus a pair state of quasineutrons, $h_{11/2}[5/2, -7/2]$. In this case the high spin states are generated by a quasiproton state $h_{11/2}[-3/2]$ plus a pair state of quasineutrons, $h_{11/2}[5/2, -7/2]$. For the ^{133}Pr isotope, the crossing occurs at $I = 15/2^-$. This crossing is represented by a 1-qp band with a configuration of a quasiproton state $h_{11/2}[-3/2]$. It is also possible to observe another crossing in high spin states ($I = 39/2^-$ to $51/2^-$), which is generated by a quasiproton state $h_{11/2}[-3/2]$ plus a pair state of quasineutrons, $h_{11/2}[5/2, -7/2]$. In this way we can observe how the PSM describes very well all yrast bands with more than one configuration in each Pr isotope.

Finally, in Fig. 6, we compare the alignment diagrams of the yrast bands obtained by the PSM with the experimental data. It is possible to observe an amount of spin alignment in each Pr isotope. This behavior is reproduced successfully by the PSM, where it explains these effects in terms of the crossing between the ground band and the 3-qp band as we have seen before. However, in the nuclei with more neutrons (^{131,133}Pr), the high spin states are not reproduced satisfactorily perhaps due to the presence of γ deformation in these nuclei.

We admit that the present calculation, while well reproducing the variation in the interaction strength at the band crossings, does not give all the observed variations of the crossing frequencies when neutron number changes (see Fig. 2). We note that precise positions (i.e., spins or rotational frequencies) where quasiparticle alignments occur are very sensitive to several calculation conditions. In the first place, correct single-particle states are important for the behavior of the aligned quasiparticle states. We note that our deformed Nilsson single-particle states are obtained by using the original Nilsson parameters [32] without any adjustment that may best suit the present nuclei. More careful choices in the input deformation parameters may also improve the agreement. We do not do such a fine tuning as far as the essential physics has been understood.

IV. CONCLUSION

The spectroscopic calculations obtained with the PSM for ^{125,127,129,131,133}Pr nuclei have allowed us to study the observed yrast bands in these odd-proton nuclei. Our calculations reveal that the dynamical moment of inertia increases its value at low frequency when N is decreased. This characteristic is related to the increase in the associated deformation in these yrast bands for the lighter isotopes.

The PSM reproduces very well the backbending phenomenon. This model proposes that this phenomenon occurs by the alignment of a 3-qp state which is formed by a quasiproton state plus a pair of quasineutron states. In conclusion, the PSM proved to be an excellent model to reproduce highly sensitive experimental data in the odd-Pr isotopes.

ACKNOWLEDGMENTS

We acknowledge financial help from DGAPA, PAEP (102301), CONACyT (México), PAPIIT (IN121809-2), and the University of Tennessee. YS was supported by the Shanghai Pu-Jiang program, the National Natural Science Foundation of China under Contract Nos. 10875077 and 11075103, and the Chinese Major State Basic Research Development Program through Grant No. 2007CB815005. Oak Ridge National Laboratory is managed by UT-Battelle, LLC, under Contract No. DE-AC05-00OR22725 with the US Department of Energy.

[1] A. Galindo-Uribarri, Rev. Mex. Fís. **45-S2**, 55 (1999).
[2] P. J. Nolan *et al.*, J. Phys. G **11**, L17 (1985).
[3] Y. Sun and M. Guidry, Phys. Rev. C **52**, R2844 (1995).
[4] M. J. Godfrey *et al.*, J. Phys. G **13**, 1165 (1987).
[5] P. K. Weng *et al.*, Phys. Rev. C **47**, 1428 (1993).
[6] C. M. Parry *et al.*, Phys. Rev. C **57**, 2215 (1998).
[7] A. N. Wilson *et al.*, Phys. Rev. C **66**, 021305 (2002).
[8] B. H. Smith *et al.*, Phys. Lett. B **443**, 89 (1998).
[9] S. M. Mullins *et al.*, Phys. Rev. C **58**, R2626 (1998).
[10] A. Galindo-Uribarri *et al.*, Phys. Rev. C **50**, R2655 (1994).
[11] A. N. Wilson *et al.*, Phys. Rev. C **63**, 054307 (2001).
[12] D. J. Hartley *et al.*, Phys. Rev. C **65**, 044329 (2002).
[13] K. Hara and Y. Sun, Int. J. Mod. Phys. E **4**, 637 (1995).
[14] I. Hamamoto, Nucl. Phys. A **271**, 15 (1976).
[15] Y. Sun, J.-Y. Zhang, and M. Guidry, Phys. Rev. Lett. **78**, 2321 (1997).
[16] Y. Sun, J.-Y. Zhang, M. Guidry, and C.-L. Wu, Phys. Rev. Lett. **83**, 686 (1999).
[17] V. Velazquez, J. Hirsch, Y. Sun, and M. Guidry, Nucl. Phys. A **653**, 355 (1999).
[18] V. Velazquez, J. Hirsch, and Y. Sun, Nucl. Phys. A **686**, 129 (2001).
[19] R. Palit, J. A. Sheikh, Y. Sun, and H. C. Jain, Phys. Rev. C **67**, 014321 (2003).
[20] R. Devi, B. D. Sehgal, S. K. Khosa, and J. A. Sheikh, Phys. Rev. C **72**, 064304 (2005).
[21] B. D. Sehgal, R. Devi, and S. K. Khosa, J. Phys. G **32**, 1211 (2006).
[22] S. Verma, P. A. Dar, and R. Devi, Phys. Rev. C **77**, 024308 (2008).
[23] Y.-C. Yang, Y. Sun, S.-J. Zhu, M. Guidry, and C.-L. Wu, J. Phys. G **37**, 085110 (2010).
[24] F. Al-Khudair, G.-L. Long, and Y. Sun, Phys. Rev. C **79**, 034320 (2009).
[25] Y. Sun, Y.-C. Yang, H.-L. Liu, K. Kaneko, M. Hasegawa, and T. Mizusaki, Phys. Rev. C **80**, 054306 (2009).

[26] V. Velazquez, J. Hirsch, and Y. Sun, Nucl. Phys. A **643**, 39 (1998).
[27] M. Dufour and A. P. Zuker, Phys. Rev. C **54**, 1641 (1996).
[28] Y. Sun and K. Hara, Comput. Phys. Commun. **104**, 245 (1997).
[29] J.-Y. Zhang, N. Xu, D. B. Fossan, Y. Liang, R. Ma, and E. S. Paul, Phys. Rev. C **39**, 714 (1989).
[30] P. Moller and J. R. Nix, At. Data Nucl. Data Tables **59**, 185 (1995).
[31] S. Rab, Nucl. Data Sheets **75**, 491 (1995).
[32] S. G. Nilsson *et al.*, Nucl. Phys. A **131**, 1 (1969).